SAMRAI: A novel variably polarized angle-resolved photoemission beamline in the VUV region at UVSOR-II

Shin-Ichi Kimura,[1,2,a)] Takahiro Ito,[1,2,b)] Masahiro Sakai,[1] Eiken Nakamura,[1] Naonori Kondo,[1] Toshio Horigome,[1] Kenji Hayashi,[1] Masahito Hosaka,[1,2,b)] Masahiro Katoh,[1,2] Tomohiro Goto,[3] Takeo Ejima,[3] and Kazuo Soda[4]
[1]*UVSOR Facility, Institute for Molecular Science, Okazaki 444-8585, Japan*
[2]*School of Physical Sciences, The Graduate University for Advanced Studies (SOKENDAI), Okazaki 444-8585, Japan*
[3]*Institute of Multidisciplinary Research for Advanced Materials, Tohoku University, Sendai 980-8577, Japan*
[4]*Graduate School of Engineering, Nagoya University, Nagoya 464-8603, Japan*

(Received 26 February 2010; accepted 15 April 2010; published online 13 May 2010)

A novel variably polarized angle-resolved photoemission spectroscopy beamline in the vacuum-ultraviolet (VUV) region has been installed at the UVSOR-II 750 MeV synchrotron light source. The beamline is equipped with a 3 m long APPLE-II type undulator with horizontally/vertically linear and right/left circular polarizations, a 10 m Wadsworth type monochromator covering a photon energy range of 6–43 eV, and a 200 mm radius hemispherical photoelectron analyzer with an electron lens of a $\pm 18°$ acceptance angle. Due to the low emittance of the UVSOR-II storage ring, the light source is regarded as an entrance slit, and the undulator light is directly led to a grating by two plane mirrors in the monochromator while maintaining a balance between high-energy resolution and high photon flux. The energy resolving power ($h\nu/\Delta h\nu$) and photon flux of the monochromator are typically 1×10^4 and 10^{12} photons/s, respectively, with a 100 μm exit slit. The beamline is used for angle-resolved photoemission spectroscopy with an energy resolution of a few meV covering the UV-to-VUV energy range. © *2010 American Institute of Physics.* [doi:10.1063/1.3425778]

I. INTRODUCTION

Angle-resolved photoemission spectroscopy (ARPES) has recently been a widely used experimental method for investigations of electronic structure as an origin of the physical properties of solids. ARPES provides information on band dispersion curves and Fermi surfaces (FSs) that cannot be obtained by other methods. The surface sensitivity of ARPES is a major issue in detecting the electronic structure of solids. When an electronic structure near the Fermi level is investigated using photons with an energy from several tens to several hundred eV, the surface electronic structure is mainly observed because the escape depth of the photoelectrons is at the subnanometer level.[1,2] For this reason, bulk-sensitive ARPES using soft- and hard-x-ray photons with an energy above several hundred eV, where the escape depth is longer than a few nanometers, has become widespread.[3,4] However, when photons in the soft- and hard-x-ray regions are used, the maximum energy resolution of ARPES is about 50 meV. If the energy resolution is comparable to the thermal broadening ($\sim 4k_BT$, where k_B is Boltzmann's constant), it is difficult to detect electronic structures revealing the origin of physical properties at temperatures lower than room temperature. Since the energy resolution of 50 meV corresponds to the thermal broadening of about 160 K, the fine electronic structure that appears at very low temperatures cannot be detected.

On the other hand, the escape depth of photoelectrons with a kinetic energy lower than 10 eV, where the excitation photon energy is below about 15 eV, is also longer than a few nanometers. In such extremely low-energy excitation, ARPES with very high-energy resolution lower than several meV and high angler resolution is available. ARPES using photons with fixed energy such as a continuous wave laser in the vacuum-ultraviolet (VUV) region, and a xenon plasma discharge lamp has also recently become available for bulk-sensitive high-resolution requirements.[5–8] On the other hand, when tunable photons such as synchrotron radiation (SR) are used for ARPES, it is able to clarify the final state effect[9] and also the overall band structure as well as the three-dimensional (3D) dispersion curve as well as the 3D position in the momentum space. The realization of a high-resolution ARPES apparatus using SR is therefore desirable.

Up to now, several VUV beamlines with very high-energy resolution have been installed around the world.[10–12] The purposes are widespread from atoms to biology. Some beamlines were designed for SR-ARPES experiment with high-energy resolution.[13–16] These SR-ARPES beamlines equip horizontally linear or helical/elliptical polarization undulators. If not only horizontally linear polarized light but also vertically polarized light are available, the symmetry of electron orbits can be defined. Then to perform high-resolution and symmetry-dependent ARPES using a variably

a)Electronic mail: kimura@ims.ac.jp.
b)Present address: Graduate School of Engineering, Nagoya University, Nagoya 464-8603, Japan.

polarized tunable photon source, we have constructed the beamline 7U, comprising a high-energy- and high-momentum-resolution ARPES beamline with variably (vertically/horizontally linear and right/left circular) polarized photons having an excitation energy of 6–43 eV at the UVSOR-II 750 MeV SR source of the Institute for Molecular Science, in Okazaki, Japan. The preliminary design concept of the beamline 7U, named Symmetry and Momentum Resolved electronic structure Analysis Instrument (SAMRAI) for functional materials, has been reported elsewhere.[17] In this paper, we report the final design of the SAMRAI beamline and the performance obtained.

II. BEAMLINE DESIGN CONCEPT

The concept of this beamline is to perform conventional ARPES measurement while maintaining a balance between high-energy resolution and high photon flux. The guideline for optics design is to achieve an energy range of 6–40 eV with a resolution of $h\nu/\Delta h\nu \sim 10^4$ and a photon flux exceeding 10^{12} photons/s on a sample with a spot size of less than 0.2×0.2 mm^2. To resolve the symmetry of electron orbitals of each band, not only horizontally but also vertically linear polarization is required. To achieve the optics requirements, an APPLE-II type undulator was adopted.

The length of the beamline on a straight line from the outgoing port is limited to about 7 m (about 12 m from the center of the undulator) due to the size of the experimental hall of UVSOR-II. However, since a normal incident mount can be used due to the required photon energy range of 6–40 eV, SR can be reflected to the direction of the storage ring. In addition, the electron beam size (2σ) of UVSOR-II is expected to be $0.08(\mathrm{V}) \times 1.08(\mathrm{H})$ mm^2 in 1% coupling machine operation because UVSOR-II was upgraded to become the lowest emittance (27 nm rad) ring among SR sources with a stored electron energy below 1 GeV in 2003.[18] The emission point can therefore be regarded as an entrance slit with a size of 80 μm when an entrance-slitless monochromator is employed. Thus the light source can be directly led to a grating without the use of prefocus mirrors, and hence a balance between high-energy resolution and high photon flux is maintained in this beamline. For these reasons, we adopted a variably polarized APPLE-II type undulator[19] and a VUV near-normal incident monochromator without an entrance slit, namely, a Wadsworth type monochromator.[13,20,21]

III. LIGHT SOURCE

To obtain variably polarized intense VUV light, an APPLE-II type undulator with a length of 3 m, periodic length λ_u=76 mm, and number of periods N=38 was adopted. Several types of undulators and multipole wigglers have been proposed to produce various polarizations up to now.[19,22–25] Among such undulators, only the APPLE-II type can produce light with horizontally/vertically linear and right/left circular polarizations. The minimum gap is 24 mm when the magnetic fields in the horizontal and vertical directions are 0.76 and 0.50 T, respectively. The lowest photon energies of the horizontally and vertically linear polarizations and the circular polarization then become 4.5, 9.7, and 7.0 eV, respectively. The calculated on-axis brilliance spectra with linearly and circularly polarized light are shown in Fig. 1. First-order light with the horizontally linear and circular polarizations covers the photon energy ranges of 4.5–50 eV and 7–50 eV, respectively. The peak brilliance of the circularly polarized light at around 35 eV reaches 1.7×10^{17} photons/s/mrad^2/mm^2/0.1%BW at a 500 mA beam current (the designed maximum beam current of UVSOR-II), which is comparable to that of third-generation SR sources.

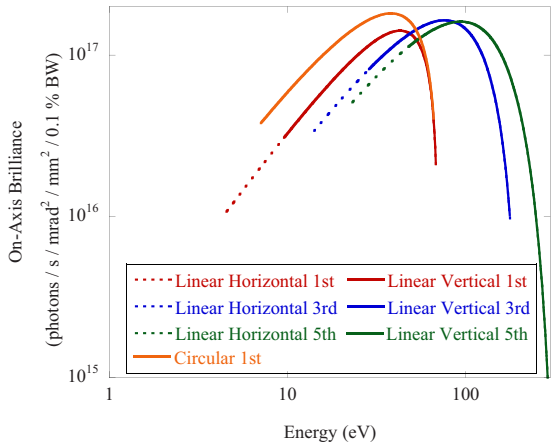

FIG. 1. (Color online) Calculated brilliance spectra of the installed APPLE-II type undulator with circular and linear polarizations at a beam current of 500 mA. 1st, 3rd, and 5th in the legend indicate degrees of harmonics. 1% coupling machine operation is assumed in the calculation.

IV. MONOCHROMATOR

We employed a Wadsworth type monochromator, which has no entrance slit, to obtain a high flux of photons. In this monochromator, the energy resolution is limited by the light source size. Since the electron beam size (2σ) at the center of the undulator is $0.08(\mathrm{V}) \times 1.08(\mathrm{H})$ mm^2 in 1% coupling operation, the energy resolution is expected to be the same as that of a monochromator with an 80 μm entrance slit. Figure 2 shows the layout of the optical components, and their characteristics are listed in Table I. The undulator light is guided to the spherical gratings (G) by two plane mirrors (M0 and M1). Since the emission angle of the undulator is small, the distance from the emission point to G must be long to irradiate the wide area of the grating. In addition, the long distance from the emission point to the grating is good for high resolution. To maintain the polarization of the undulator radiation, the incident angles of M0 and M1 are set at 85° and 7.5°, respectively.

The heat load from the undulator radiation is reduced by M0 and M1, which are equipped with water-cooling systems. M0 and M1 mainly reduce the heat load from the high- and low-energy photons, respectively. The direction and position of the undulator radiation to the gratings (G) can be controlled by these two mirrors. In general, normally incident mirrors lose photon flux at higher energy regions because the reflectivity of materials decreases with increasing photon energy. To obtain high photon flux in the whole energy region of 6–40 eV, M1 is an interchangeable mirror system, com-

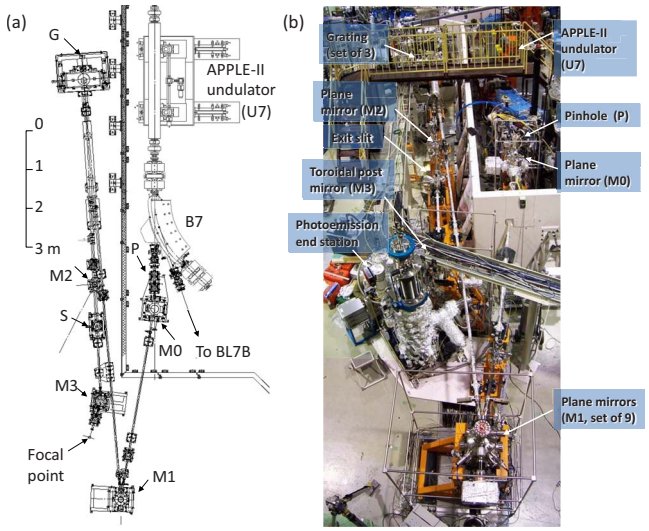

FIG. 2. (Color online) Layout (a) and photograph (b) of the SAMRAI beamline consisting of the APPLE-II type undulator (U7), the modified Wadsworth type monochromator (M0-S), and the high-resolution photoemission analyzer at the focal point. The monochromator mainly has five optical components: two plane mirrors (M0 and M1) with water cooling, one set of three spherical gratings (g), an exit slit (s), and one toroidal refocusing mirror (M3). The spherical gratings with a radius of 10 m are located 22 m from the center of the undulator. There is no entrance slit. S is located 6.47 m from G. A second branch for a VUV microscope end station is planned to be constructed after the plane mirror (M2) located between G and S.

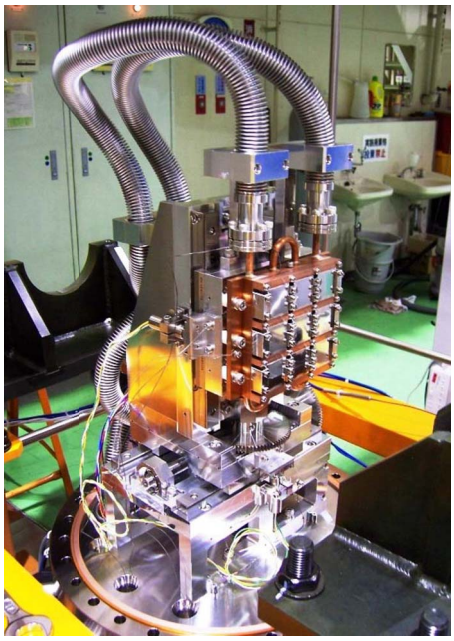

FIG. 3. (Color online) Nine mirrors of M1 with water cooling.

posed of eight plane mirrors of one Au-coated Si substrate, two SiC, one Si, and four Mg/SiC multilayer mirrors and one blank as shown in Fig. 3. The mirrors can be set and aligned on the light axis by pulse motors without breaking the vacuum. The reflectivity of Au, SiC, and Si mirrors rapidly decreases with increasing photon energy above 25 eV,[26] while the Mg/SiC multilayer mirrors mainly cover the region above 29 eV.[27] A detailed explanation is given later.

The gratings (G) are set 11 m from M1 (22 m from the center of the undulator), as shown in Fig. 2. Three spherical gratings of 10 m in radius with a constant grooving density of 3600 (G1), 2400 (G2), and 1200 (G3) lines/mm optimized at the photon energies of 32, 20, and 10 eV, respectively, were adopted. For high reflectivity in the energy region below 15 eV, G3 is coated with SiC, while the coated material of G1 and G2 is Au. The gratings move not only rotationally to select the photon energy but also translationally to focus the monochromatized light on the exit slit (S) located 6.47 m from G with an off-axis angle of 1°, similar to an off-plane Eagle type monochromator.[28] Since the distance between G and S is about 0.3 times that between the center of the undulator and G, the size of the light on the exit slit is reduced to 0.3 times the size of the electron beam. The off-axis angle of G of 1° maintains almost the same focal length between the horizontal and vertical directions. Therefore, the beam shape on the exit slit is almost the same as that of the stored electron beam in the storage ring. A MgF_2 filter is installed after S for avoiding higher-order lights when photons below 10 eV are used.

The postfocus toroidal mirror (M3) is located 2 m from the exit slit and focuses the monochromatized light to a sample in the ARPES end station located 1 m from M3. The

TABLE I. Characteristics of optical components of the Wadsworth monochromator in the SAMRAI beamline. The size of mirrors indicates length × width × height. r_l and r_s of mirror 3 (M3) indicate the radii of longitudinal and sagittal focuses, respectively.

		Distance from emission point (m)	Size	Shape	Horizontal incident angle (°)	Material
Pinhole	(P)	5.4	0.1, 0.2, 0.4, 1.0, 2.0, 4.0, and 8.0 mm dia.	···	···	Cu
Mirror	(M0)	6.0	$100\times30\times20$ mm^3	Plane	85	Au on Si
Mirror	(M1)	11.0	$25.4\times25.4\times10$ mm^3	Plane	7.5	Au on Si, SiC, Si, and Mg/SiC multilayers
Grating	(G1)	22.0	$30\times30\times10$ mm^3	Spherical (r=10 m, 3600 lines/mm)	1	Au on SiO_2
	(G2)	22.0	$30\times30\times10$ mm^3	Spherical (r=10 m, 2400 lines/mm)	1	Au on SiO_2
	(G3)	22.0	$30\times30\times10$ mm^3	Spherical (r=10 m, 1200 lines/mm)	1	SiC on SiO_2
Mirror	(M2)	27.4	$50\times20\times10$ mm^3	Plane	75	Au on SiO_2
Exit slit	(S)	28.67	3–500 μm	···	···	SUS/BeCu
Mirror	(M3)	30.67	$100\times15\times10$ mm^3	Toroidal (r_l=7678.4 mm and r_s=231.5 mm)	80	Au on SiO_2

TABLE II. Design parameters for Mg/SiC wide-band multilayers in the 30–40 eV photon energy region.

Multilayer Number	Number of periods	Period length D (nm)	Thickness ratio $\gamma=d_{SiC}/D$
1	7	16.6	0.42
2	7	18.0	0.41
3	6	19.8	0.40
4	6	22.2	0.40

size of the light is reduced to half the size of the beam on the exit slit. Since the beam size at S is reduced to 0.3 times the size of the electron beam by the asymmetric configuration of the monochromator in addition to the reduction ratio of 0.5 due to M3, the size of the light on the sample is ideally reduced by 15% from the electron beam size, i.e., 160(H) $\times$12(V) μm^2.

One plane mirror (M2) is installed in between G and S. The mirror guides the monochromatized light to a second branch mainly used for a VUV microscope through another exit slit. The end station is not permanent and users can bring their own experimental chamber.

All of the chambers containing optical components are located in plastic housings to maintain stable temperature.

A. Multilayer mirrors

To increase the throughput intensity and reduce higher-order light in the energy region higher than 30 eV, we adopted Mg/SiC multilayer mirrors for M1. Multilayers for near-normal incidence (7.5° from the normal direction) were designed to increase the bandwidth while maintaining the reflectivity in the 29–43 eV photon energy region. The material pair chosen for the multilayer mirrors was an Mg/SiC pair, which is known to show high reflectance in this photon energy region.[27] The fabricated multilayers were designed using the layer-by-layer method except for periodic numbers.[29] The periodic numbers were decreased to enlarge the reflection band width. The obtained design parameters are listed in Table II, and the calculated reflectivity spectra using these parameters are shown as lines in Fig. 4. The multilayers were deposited on Si substrates [25.4(L) $\times$25.4(W)$\times$10(H) mm^3] for the M1 mirrors by using a conventional magnetron sputtering system (SPL-500, Canon ANELVA Co., Japan). For evaluation of the fabricated multilayer mirrors, the multilayers were deposited simultaneously on Si wafers. The deposition rates were controlled to maintain constant periodic lengths of the multilayers in the mirror area. The deposition rate of Mg was 5.8 nm/min and that of SiC deposition was 0.87 nm/min on average. The error of the periodic lengths of the fabricated multilayers was $\pm$2% in the mirror area estimated from x-ray diffraction measurements. Reflectivity measurements were performed at the instrument calibration beamline 5B of UVSOR-II with an energy resolving power $h\nu/\Delta h\nu$ of about 200. The obtained spectra are shown as marks in Fig. 4. The peak reflectivities of the multilayers are about 0.3, which is consistent with the calculation. The four fabricated multilayer mirrors cover the 29–43 eV photon energy region with a reflectivity of 0.15 or higher.

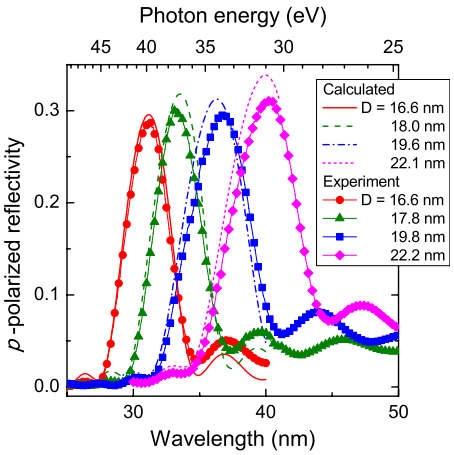

FIG. 4. (Color online) Calculated and experimentally obtained *p*-polarized reflectivity spectra with an incident angle of 7.5° of Mg/SiC multilayer mirrors installed at M1. These mirrors are optimized at photon energies of 31, 34, 37, and 40 eV.

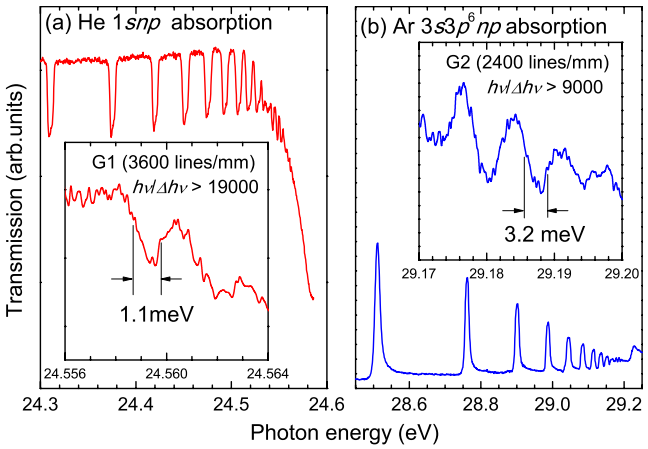

FIG. 5. (Color online) Transmission spectra of helium 1*snp* absorption and argon $3s3p^6np$ window-type resonance measured with the G1 and G2 gratings, respectively, and an exit slit size of 100 μm. The energy resolving powers $h\nu/\Delta h\nu$ were evaluated as 19 000 at 24.56 eV for G1 and 9000 at 29.19 eV for G2.

B. Obtained resolution and photon flux

The energy resolving power and photon flux under the same monochromator conditions with an exit slit size of 100 μm were checked when the storage ring was operated with a 3% coupling constant. The energy resolving power was tested by measuring absorption spectra of rare gases. The typical transmission spectra of helium 1*snp* ($h\nu$: $\sim$24.5 eV) absorption and argon $3s3p^6np$ ($h\nu$: $\sim$29 eV) window-type resonance[30] are shown in Fig. 5. The helium absorption spectrum was recorded using G1 (3600 lines/mm) for the highest energy range. Since the absorption line with the peak width of 1.1 meV can be resolved, the energy resolving power was evaluated as $h\nu/\Delta h\nu \geq 19\,000$. On the other hand, the argon spectrum (peak width: 3.2 meV) was obtained with G2 (2400 lines/mm), and the energy resolving power was evaluated as $h\nu/\Delta h\nu \geq 9000$. The obtained and geometrically calculated energy resolving powers are plotted in Fig. 6. The energy

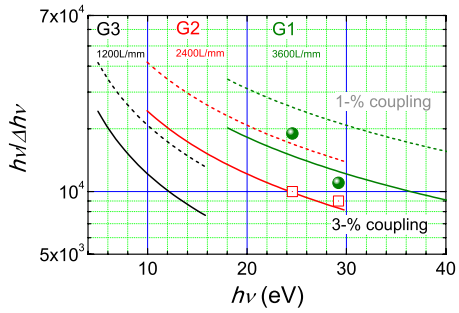

FIG. 6. (Color online) Theoretical energy resolving power $h\nu/\Delta h\nu$ with 1% (dashed lines) and 3% (solid lines) coupling constants of storage ring operation. The experimentally obtained energy resolving powers at 24.5 and 29.2 eV with G1 (solid circles) and G2 (open squares) with a 3% coupling constant are also plotted.

resolving power of this beamline depends on the electron beam parameters of the storage ring, particularly the beam size at the emission point. Both of the energy resolving powers obtained at 24.5 and 29 eV is located at the theoretical ones for the 3% coupling constants. Therefore, the experimental energy resolving power is a reasonable value. In the near future, UVSOR-II will be operated in the top-up mode and the coupling constant will be reduced to the ideal value of 1%, whereupon the energy resolving power will become 1.7 times higher than the present level with the same photon flux.

Using the same beamline parameters, the photon flux was detected using a calibrated silicon photodiode (AXUV100, International Radiation Detectors, Inc., USA[31]). The results are shown in Fig. 7. The spectra were recorded using the typical combinations of undulator gap, M1 mirrors, and gratings. The photon flux in the region of 7–11 eV for G3 and 15–23 eV for G2 exceeds 10^{12} photons/s at the stored beam current of 300 mA. In the energy region above 25 eV using G2, the intensity rapidly decreases with increasing photon energy because of the poor reflectivity of the Au mirror in M1. In the energy region above 25 eV, the four Mg/SiC multilayer mirrors described earlier can be used. Since the reflectivity is several tens of times higher than that

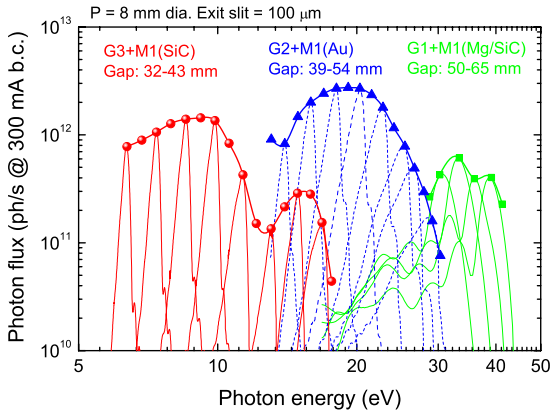

FIG. 7. (Color online) Obtained photon flux spectra (solid and dashed lines) with a 100 μm exit slit ($h\nu/\Delta h\nu$ of $\sim 10^4$ is roughly expected) of the combination of gratings, M1 mirrors, and undulator gap size. The marked lines are the trace of the peak intensity of the solid and dashed lines.

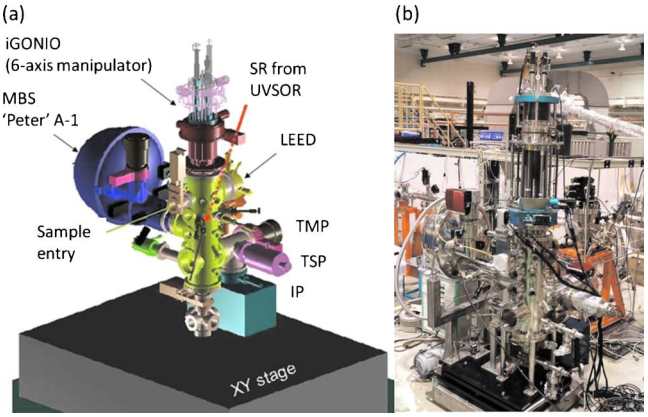

FIG. 8. (Color online) Schematic figure (a) and photograph (b) of the ARPES end station at the SAMRAI beamline (BL7U). The end station is equipped with a photoelectron analyzer (A-1 analyzer), a six-axis manipulator with a liquid-helium-flow type cryostat (i-GONIO virtual-shaft type) and a low-energy electron diffraction device to check sample rotation. Three pumps [turbo molecular pump (TMP), titanium sublimation pump (TSP), and ion pump (IP)] are used for making an ultrahigh vacuum.

of Au film in the energy region, the photon flux will recover to at least 3×10^{11} photons/s.

V. PHOTOEMISSION END STATION

The beamline has two branches. One is an ARPES end station for solids, and the other is for a VUV microscope, which is guided by the M2 mirror as shown in Fig. 2. Figure 8 shows a schematic figure and photograph of the ARPES end station.

The main part of the ARPES apparatus consists of a 200 mm radius hemispherical photoelectron energy analyzer with a wide-angle electron lens (A-1 analyzer, MB Scientific AB, Sweden) located at 50° from the incident undulator radiation, and a liquid-helium-flow cryostat with a six-axis manipulation system (i-GONIO virtual-shaft-type, A-VC, R-DEC Co., Japan).[32] To obtain ARPES spectra along the high-symmetry lines of a sample, the sample manipulator is equipped with three independent rolling mechanisms; two of these are rotations [θ_x for horizontal angle (angular direction) and θ_y for vertical angle (energy direction)] with respect to the sample surface normal, and the other is an in-plane rotation (ϕ). The maximum rotational angles are $\pm50°$ for θ_x, +55° and −5° for θ_y, and $\pm10°$ for ϕ due to the geometrical limitation. In addition, to permit a complete data set to be obtained, not only of FS mapping but also of quasiparticle band dispersion within 12 h (the typical user beam operation time of UVSOR-II in a day), a computational multidimensional scanning system is developed.

A wide-acceptance electron lens is installed in the photoelectron analyzer. To check the acceptance angle and angular resolution of the electron lens, we developed an angular-distribution test device, shown in Fig. 9(c). This device consists of a tungsten wire 60 μm in diameter and a transmission grating with 250 μm spacing. The angular image shown in Figs. 9(a) and 9(b) has a separation of 1°. The angular image was recorded using the zeroth light of the undulator radiation set at $h\nu$=10 eV. From the angular image, the maximum acceptance angle is found to be ±18°,

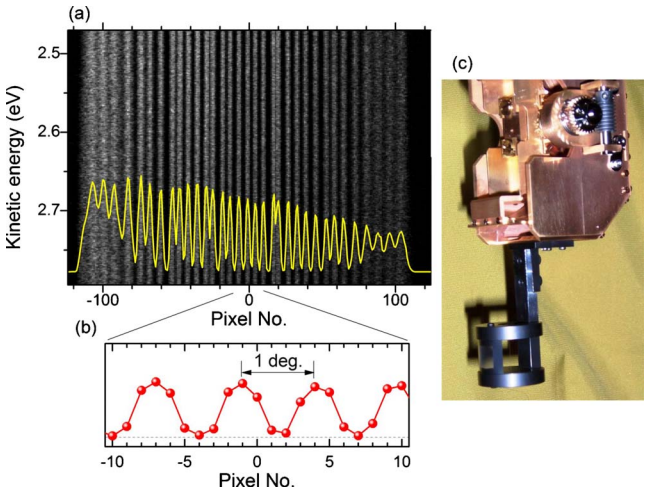

FIG. 9. (Color online) (a) Angular distribution of photoelectrons of the angular-distribution test device at a kinetic energy of 2.47–2.794 eV excited by an undulator radiation of 10 eV. The angular space is 1°. The total acceptance angle of the analyzer is ±18°. (b) Magnified angular distribution of (a) near the center of the pixels. 1° consists of 5 pixels (0.2°/pixel). (c) Photo of the angular-distribution test device installed at the bottom of the sample manipulator.

and the angle resolution is better than 0.2°. An irregularly spaced angular distribution is observed because of the diffraction and/or aberrations in the electron lens of the photoelectron analyzer at the low kinetic energy, although a uniform angular distribution appears when higher kinetic photoelectrons are detected (not shown). This means that obtained ARPES images of samples must be calibrated using the test device. The test device is permanently installed at the bottom of the sample manipulator.

A. Energy resolution of photoemission spectroscopy at the SAMRAI beamline

We briefly introduce the present photoemission spectroscopy measurement performance. The energy resolution was evaluated by using the measurement of an Au Fermi-edge spectrum (solid circles) at a sample temperature of 15 K (the accessible lowest temperature of the cryostat at present) as shown in Fig. 10. The excitation photon energy was set to be 10 eV. In the measurement, frequently used parameters for angle-integrated photoemission measurements (horizontal planar polarization, monochromator slit size of 50 μm, analyzer pass energy of 2 eV, analyzer slit size of 0.2 mm, and spatial mode) are adopted. The dashed line superimposed on the data shows a simulated Fermi edge, obtained as a Gaussian function of 2 meV full width at half maximum (FWHM) convolved with the Fermi–Dirac distribution function (solid line) of 15 K. The total energy resolution (ΔE_{total}) can be evaluated as less than 2 meV from FWHM of the Gaussian function. The obtained ΔE_{total} is almost consistent with the designed ΔE_{total} of 1.5 meV from the designed energy resolutions of the monochromator of 0.83 meV (3% coupling constant) and of the analyzer of 1.2 meV (pass energy of 2 eV, slit size of 0.2 mm). The horizontal spot size on the sample is about 0.2 mm or less that is consistent with the designed value.

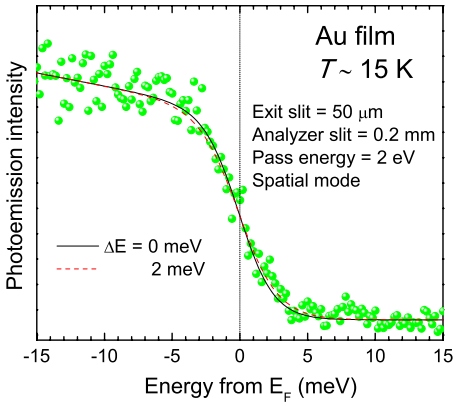

FIG. 10. (Color online) An energy distribution curve (solid circles) of the Fermi cutoff of an evaporated Au film measured at the SAMRAI beamline using the excitation photon energy of 10 eV. The dashed line is a simulated Fermi edge obtained as a Gaussian function of 2 meV FWHM convoluted with the Fermi–Dirac distribution function (solid line) at 15 K. The total energy resolution was evaluated as less than 2 meV. Some of the parameters for the measurement are indicated in the figure.

B. Example of ARPES measurement

Figure 11 shows a 3D ARPES result for the strongly correlated $4f$ electron compound CeSb. CeSb is a suitable material for checking the performance of 3D band dispersions as well as FS because of its well-known band structure,[33] and a number of ARPES studies have been performed so far.[34–36] The main purpose in this study is to demonstrate that the 3D FS of CeSb in the paramagnetic phase can be elucidated by using the SAMRAI beamline. By tuning of the sample tilting (θ_y) as well as the photon energy, we have successfully mapped out the topology of cigar-shaped holelike FS at the X point, which is well reproduced by the band calculation (3D illustration in Fig. 11). It should be noted that the time required for acquisition of the present 3D FS image together with the 3D band structure is within 6 h. The present high-throughput measurement can be realized by the abundance of high photon flux at the SAMRAI beamline as well as the six-axis sample manipulation system. These results clearly indicate that VUV 3D ARPES provides detective information on bulk 3D electronic structures that can be

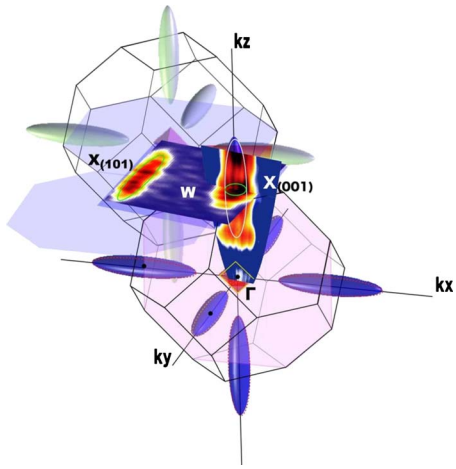

FIG. 11. (Color online) 3D FS image of CeSb measured at the SAMRAI beamline.

compared with band calculations. The detailed analysis, for instance, the different shape of FSs in the k_x-k_z plane from that in the k_x-k_y plane, is discussed elsewhere.[37]

VI. CONCLUSION

We reported the design and performance in the VUV region with variably polarized high-flux photons of a novel high-energy resolution angle-resolved photoemission beamline, SAMRAI, constructed at the UVSOR-II facility at the Institute for Molecular Science, Japan. The beamline is equipped with an APPLE-II type undulator as a light source, a Wadsworth type monochromator, and a photoemission end station with a 200 mm radius hemispherical photoelectron analyzer with a $\pm 18°$ acceptance angle. The beamline successfully maintains a balance between high photon energy resolving power ($h\nu/\Delta h\nu$: $\sim 10^4$) and high photon flux ($\sim 10^{12}$ photons/s), which is consistent with ray-tracing calculations. The total energy resolution of a typical ARPES measurement parameter at the excitation photon energy of 10 eV is 1.5 meV that is consistent with the designed value. The beamline is now in operation and is available to users from around the world.

ACKNOWLEDGMENTS

We would like to thank UVSOR staff members, especially Professor N. Kosugi and Professor E. Shigemasa, for their support and assistance. We also thank Dr. P. Baltzer and Ms. M. Matsuki-Baltzer for providing the transmission grating for the angular-distribution test device and their fruitful suggestions and Dr. Miyazaki, Mr. Hajiri, and Mr. Mitani for taking data in Figs. 9 and 10. This work was supported by a joint studies program of the Institute for Molecular Science (2006–2009).

[1] M. P. Seah and W. A. Dench, Surf. Interface Anal. **1**, 2 (1979).
[2] S. Tanuma, C. J. Powell, and D. R. Penn, Surf. Interface Anal. **21**, 165 (1994).
[3] A. Sekiyama, T. Iwasaki, K. Matsuda, Y. Saitoh, Y. Ônuki, and S. Suga, Nature (London) **403**, 396 (2000).
[4] Y. Takata, K. Tamasaku, T. Tokushima, D. Miwa, S. Shin, T. Ishikawa, N. Yabashi, K. Kobayashi, J. J. Kim, T. Yao, T. Yamamoto, M. Arita, H. Namatame, and M. Taniguchi, Appl. Phys. Lett. **84**, 4310 (2004).
[5] T. Kiss, T. Shimojima, F. Kanetaka, K. Kanai, T. Yokoya, S. Shin, Y. Ônuki, T. Togashi, C. Q. Zhang, C. T. Chen, and S. Watanabe, J. Electron Spectrosc. Relat. Phenom. **144–147**, 953 (2004).
[6] T. Kiss, T. Shimojima, K. Ishizaka, A. Chainani, T. Togashi, T. Kanai, X.-Y. Wang, C.-T. Chen, S. Watanabe, and S. Shin, Rev. Sci. Instrum. **79**, 023106 (2008).
[7] S. Souma, T. Sato, T. Takahashi, and P. Baltzer, Rev. Sci. Instrum. **78**, 123104 (2007).
[8] G. Funabashi, H. Fujiwara, A. Sekiyama, M. Hasumoto, T. Ito, S. Kimura, P. Baltzer, and S. Suga, Jpn. J. Appl. Phys. **47**, 2265 (2008).
[9] T. Yamasaki, K. Yamazaki, A. Ino, M. Arita, H. Namatame, M. Taniguchi, A. Fujimori, Z.-X. Shen, M. Ishikado, and S. Uchida, Phys. Rev. B **75**, 140513(R) (2007).
[10] P. A. Heimann, M. Koike, C.-W. Hsu, D. Blank, X. M. Yang, A. G. Suits, Y. T. Lee, M. Evans, C. Y. Ng, C. Flaim, and H. A. Padmore, Rev. Sci. Instrum. **68**, 1945 (1997).
[11] G. Reichardt, J. Bahrdt, J.-S. Schmidt, W. Gudat, A. Ehresmann, R. Müller-Albrecht, H. Molter, H. Schmoranzer, M. Martins, N. Schwentner, and S. Sasaki, Nucl. Instrum. Methods Phys. Res. A **467–468**, 462 (2001).
[12] A. Giuliani, F. Jamme, V. Rouam, F. Wien, J.-L. Giorgetta, B. Lagarde, O. Chubar, S. Bac, I. Yao, S. Rey, C. Herbeaux, J.-L. Marlats, D. Zerbib, F. Polack, and M. Réfrégiers, J. Synchrotron Radiat. **16**, 835 (2009).
[13] J. Bisognano, M. Severson, M. A. Green, G. Rogers, M. Fisher, T. Kubala, and M. Bissen, Nucl. Instrum. Methods Phys. Res. A **467–468**, 492 (2001).
[14] T. Matsui, H. Sato, K. Shimada, M. Arita, S. Senba, H. Yoshida, K. Shirasawa, M. Morita, A. Hiraya, H. Namatame, and M. Taniguchi, Nucl. Instrum. Methods Phys. Res. A **467–468**, 537 (2001).
[15] L. Petaccia, P. Vilmercati, S. Gorovikov, M. Barnaba, A. Bianco, D. Cocco, C. Masciovecchio, and A. Goldoni, Nucl. Instrum. Methods Phys. Res. A **606**, 780 (2009).
[16] M. H. Berntsen, P. Palmgren, M. Leandersson, A. Hahlin, J. Åhlund, B. Wannberg, M. Månsson, and O. Tjernberg, Rev. Sci. Instrum. **81**, 035104 (2010).
[17] S. Kimura, T. Ito, E. Nakamura, M. Hosaka, and M. Katoh, AIP Conf. Proc. **879**, 527 (2007).
[18] M. Katoh, M. Hosaka, A. Mochihashi, J. Yamazaki, K. Hayashi, Y. Hori, T. Honda, K. Haga, Y. Takashima, T. Koseki, S. Koda, H. Kitamura, T. Hara, and T. Tanaka, AIP Conf. Proc. **705**, 49 (2004).
[19] S. Sasaki, K. Miyata, and T. Takada, Jpn. J. Appl. Phys., Part 2 **31**, L1794 (1992).
[20] C. R. Howle, S. Ali, R. P. Tuckett, D. A. Shaw, and J. B. West, Nucl. Instrum. Methods Phys. Res. B **237**, 656 (2005).
[21] R. T. Wegh and A. Meijerink, Phys. Rev. B **60**, 10820 (1999).
[22] T. Tanaka and H. Kitamura, J. Synchrotron Radiat. **3**, 47 (1996).
[23] S. Yamamoto, H. Kawata, H. Kitamura, M. Ando, N. Saki, and N. Shiotani, Phys. Rev. Lett. **62**, 2672 (1989).
[24] H. Onuki, N. Saito, T. Saito, and M. Habu, Rev. Sci. Instrum. **60**, 1838 (1989).
[25] S. Kimura, M. Kamada, H. Hama, X. M. Maréchal, T. Tanaka, and H. Kitamura, J. Electron Spectrosc. Relat. Phenom. **80**, 437 (1996).
[26] E. D. Palick, *Handbook of Optical Constants of Solids* (Academic, New York, 1985).
[27] T. Ejima, A. Yamazaki, T. Banse, K. Saito, Y. Kondo, S. Ichimaru, and H. Takenaka, Appl. Opt. **44**, 5446 (2005).
[28] T. Namioka, J. Opt. Soc. Am. **49**, 460 (1959); **49**, 961 (1959).
[29] M. Yamamoto and T. Namioka, Appl. Opt. **31**, 1622 (1992).
[30] R. P. Madden, D. L. Ederer, and K. Codling, Appl. Opt. **6**, 31 (1967).
[31] E. M. Gullikson, R. Korde, L. R. Canfield, and R. E. Vest, J. Electron. Spectrosc. Relat. Phenom. **80**, 313 (1996).
[32] Y. Aiura, H. Bando, T. Miyamoto, A. Chiba, R. Kitagawa, S. Maruyama, and Y. Nishihara, Rev. Sci. Instrum. **74**, 3177 (2003).
[33] Y. Kaneta, S. Iwata, T. Kasuya, and O. Sakai, J. Phys. Soc. Jpn. **69**, 2559 (2000).
[34] H. Kumigashira, H.-D. Kim, A. Ashihara, A. Chainani, T. Yokoya, T. Takahashi, A. Uesawa, and T. Suzuki, Phys. Rev. B **56**, 13654 (1997).
[35] T. Ito, S. Kimura, and H. Kitazawa, Physica B **351**, 268 (2004).
[36] A. Takayama, S. Souma, T. Sato, T. Arakane, and T. Takahashi, J. Phys. Soc. Jpn. **78**, 073702 (2009).
[37] T. Ito, S. Kimura, and H. Kitazawa (unpublished).